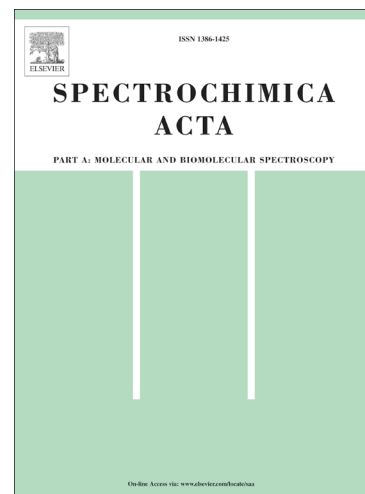


Journal Pre-proofs

Combined spectroscopic and theoretical analysis of the binding of a water-soluble perylene diimide to DNA/RNA polynucleotides and G-quadruplexes

Francesca Macii, Lorenzo Cupellini, Mariassunta Stifano, Javier Santolaya, Cristina Pérez-Arnaiz, Andrea Pucci, Giampaolo Barone, Begoña García, Natalia Busto, Tarita Biver

PII: S1386-1425(21)00490-X
DOI: <https://doi.org/10.1016/j.saa.2021.119914>
Reference: SAA 119914



To appear in: *Spectrochimica Acta Part A: Molecular and Biomolecular Spectroscopy*

Received Date: 9 February 2021
Revised Date: 23 April 2021
Accepted Date: 2 May 2021

Please cite this article as: F. Macii, L. Cupellini, M. Stifano, J. Santolaya, C. Pérez-Arnaiz, A. Pucci, G. Barone, B. García, N. Busto, T. Biver, Combined spectroscopic and theoretical analysis of the binding of a water-soluble perylene diimide to DNA/RNA polynucleotides and G-quadruplexes, *Spectrochimica Acta Part A: Molecular and Biomolecular Spectroscopy* (2021), doi: <https://doi.org/10.1016/j.saa.2021.119914>

This is a PDF file of an article that has undergone enhancements after acceptance, such as the addition of a cover page and metadata, and formatting for readability, but it is not yet the definitive version of record. This version will undergo additional copyediting, typesetting and review before it is published in its final form, but we are providing this version to give early visibility of the article. Please note that, during the production process, errors may be discovered which could affect the content, and all legal disclaimers that apply to the journal pertain.

Combined spectroscopic and theoretical analysis of the binding of a water-soluble perylene diimide to DNA/RNA polynucleotides and G-quadruplexes

Francesca Macii,¹ Lorenzo Cupellini,¹ Mariassunta Stifano,¹ Javier Santolaya,^{1,3} Cristina Pérez-Arnaiz,² Andrea Pucci,¹ Giampaolo Barone,³ Begoña García,² Natalia Busto,^{2*} Tarita Biver^{4,1*}

¹ Department of Chemistry and Industrial Chemistry, University of Pisa, Via G. Moruzzi 13, 56124 Pisa, Italy

² Department of Chemistry, University of Burgos, Pza. Misael Bañuelos s/n, 09001 Burgos, Spain
nbusto@ubu.es

³ Department of Biological, Chemical and Pharmaceutical Sciences and Technologies, University of Palermo, Viale delle Scienze Ed. 17, 90128 Palermo, Italy

⁴ Department of Pharmacy, University of Pisa, Via Bonanno Pisano 6, 56126 Pisa, Italy, tarita.biver@unipi.it

Keywords

Density functional theory, intercalation, sitting atop, molecular dynamics, aggregation

Abstract

We present here a combined spectroscopic and theoretical analysis of the binding of N,N'-bis(2-(1-piperazino)ethyl)-3,4,9,10-perylenetetracarboxylic acid diimide dichloride (PZPERY) to different biosubstrates. Absorbance titrations and circular dichroism experiments, melting studies and isothermal calorimetry (ITC) titrations reveal a picture where the binding to natural double-stranded DNA is very different from that to double and triple-stranded RNAs (poly(A)-poly(U) and poly(U)-poly(A)□poly(U)). As confirmed also by the structural and energetic details clarified by density functional theory (DFT) calculations, intercalation occurs for DNA, with a process driven by the combination of aggregates disruption and monomers intercalation. Oppositely, for RNAs, no intercalation but groove binding with the formation of supramolecular aggregates is observed. Among all the tested biosubstrates, the affinity of PZPERY towards DNA G-quadruplexes (G4) is the greatest one with a preference for human telomeric G4s. Focusing on hybrid G4 forms, either sitting-atop ("tetrad-parallel") or lateral ("groove-parallel") binding modes were considered in the discussion of the experimental results and molecular dynamics (MD) simulations. Both turned out to be possible concurrently, in agreement also with the experimental binding stoichiometries higher than 2:1.

1. Introduction

Perylene diimides (PDIs) derivatives are aromatic dyes which show intense visible light absorption, excellent photostability and high quantum yields. The low reduction potential of PDIs [1] makes them electron acceptors and semiconductors in photoinduced charge transfer reactions; that's why they are studied for applications in the fields of energy storage and photovoltaics [2],[3], luminescent solar concentrators [4], OLEDs [5], nano-scale electronic components [6] and nano-sensors [7]. PDIs undergo auto-aggregation, and the aggregates show interesting new photophysical properties arising from π - π coupling [8],[9],[10]. The absorbance and emission features of PDIs can be used for sensing purposes [11],[12],[13],[14]. From the biochemical point of view, PDIs can interact with double-stranded DNA (dsDNA) both by the formation of extended aggregates on the external DNA backbone [15] or by intercalating between the DNA base pairs [16]. Small molecular size and the strong polarity of hydrophilic substituents are prerequisites for PDI-based DNA intercalators [17]. As from the sensing point of view, PDI-engineered DNA strands may undergo rapid electron transfer reactions that could serve as a signal reporter for fluorescent nucleic acid detection [18]. Also, Biotin-PDI molecules were found to be an effective method for fishing G-quadruplex (G4) structures using streptavidin coated magnetic beads [19]. PDIs derivatives might have anti-tumour properties, as they were found to be involved in the inhibition of the telomerase activity by stabilizing DNA-G4s [20]. For instance, the landmark N,N'-bis-(2-(1-piperidino)ethyl)-3,4,9,10-perylene tetracarboxylic acid diimide (PIPER) and derivatives were proposed to be promising G4 binders with a selectivity over dsDNA which depends on pH and on self-aggregation tendency [21],[22]. N,N'-bis-{4-[1-oxo-6-biotinamidohexyl]piperidin-4-yl}-1,6,7,12-tetrakis[3,5-bis(hydroxycarbonyl)phenoxy]-perylene-3,4,9,10-tetracarboxylic diimide was found to interact with G4 structures with high selectivity, as no affinity towards double helix DNA was displayed [19]. PDI derivatives have been found to promote the formation of G4s from oligonucleotides [23],[24] and even to shift G4 conformation from one to another [25]; in these studies it is also shown that the electrostatic interactions of the side chains with the grooves play a role in selecting the G4 topology and producing a different ability to inhibit telomerase. The role of different PDI side-chains in the G4 binding process was further characterised [26],[27],[28]. Positive charges emerged to be significantly involved in the G4 stabilization as the PDI bearing positively charged substituents was found to inhibit the telomerase activity to a greater extent with respect to the neutral equivalents [29]. Also, the distance between the charged nitrogen atoms in the side-chains and the aromatic moiety of PDI is known to be an important parameter, in particular, to optimize the interactions with the negatively charged sugar-phosphate backbone. This evidence is in agreement with the binding model proposed by Hurley and co-workers, according to whom planar ligands are generally stacked on the terminal G-tetrad of the quadruplex [30]. This is shown also in papers concerning PDI derivatives [31]. However, the G-tetrad may also be hindered, and different conformations will drive formation of adducts with different geometries and ligand/DNA binding stoichiometries larger than 1:1 [25]. On the whole, PDI's structure/behaviour relationships are not always fully explored and mechanistic insights into the direct interaction with biosubstrates are not always available.

A robust knowledge of the details of the molecular interactions could be very important to develop new efficient therapeutic agents and sensors [32]. In this study, we combined spectroscopic and theoretical investigations to understand PDI derivative binding to nucleic acids. To the best of our

knowledge, just a few examples of MD simulations for G4 binding are reported in the literature [19],[33],[25] whereas no DFT calculation on DNA/PDI derivatives is reported at all. As for MD simulations, the PDB entries used often refer to parallel or anti-parallel G4 structures with inner G-tetrad accessibility [34],[35]; as this accessibility may not always be ensured in real/hybrid systems it might be interesting to check what happens in the case of more hindered conformations. The binding to double helix RNA is scarcely investigated [36],[37], while information on the binding to triple helix RNA is missing at all; data on intercalation are often based on qualitative approaches [17],[16] and the same may hold sometimes for G4 binding studies where the spectroscopic results are not quantitatively discussed [28]. On this basis, and given the still high and even increasing interest for cutting-edge applications of these systems [12],[38], we think there is room for a combined spectroscopic/computational investigation, to provide binding details of a PDI compound to poly- and oligonucleotides. On this basis, the water soluble N,N'-bis(2-(1-piperazino)ethyl)-3,4,9,10-perylenetetracarboxylic acid diimide dichloride (PZPERY, Figure 1) is here tested to get information on the mechanistic aspects of its binding to double-stranded DNA, G4 DNAs and RNA both in double and triple helix forms.

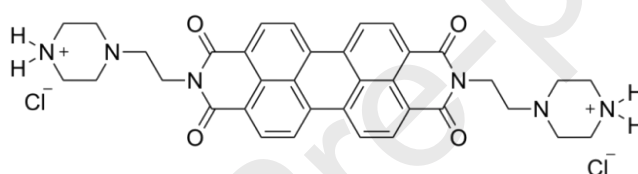


Figure 1. Molecular structure of N,N'-bis(2-(1-piperazino)ethyl)-3,4,9,10-perylenetetracarboxylic acid diimide dichloride (PZPERY).

2. Materials and Methods

2.1 Materials For the synthesis of N,N'-bis(2-(1-piperaziny)ethyl)-3,4,9,10-perylenetetracarboxylic acid diimide dichloride (PZPERY) please refer to refs. [7] and [39]; some details are also provided in the Supporting Information. PZPERY peripheral chains are composed by piperazine rings (first pKa = 9.1 – 9.2 for alkyl piperazines [40]), that are considered fully charged in the selected physiological conditions. Stock solutions of PZPERY were prepared by weight directly in the aqueous buffer needed (see below) and kept at 4°C in the dark. Calf thymus DNA (lyophilised sodium salt from Sigma-Aldrich, from now on ct-DNA) was dissolved in water and sonicated, producing short polynucleotide fragments (ca. 500 base pairs) [41]. The sonication procedure used a MSE-Sonyprep sonicator and 7 cycles of 10 s sonication + 20 s pause at 14 μ m amplitude; each sonicated aliquot (8 mL) was kept in ice bath and the final strand length was checked by agarose electrophoresis using a 100 bp DNA ladder. Then, small stock ct-DNA aliquots (1.5 mL vial) were frozen and melted just before use. Stock solutions of ct-DNA were standardized spectrophotometrically ($\epsilon = 13200 \text{ M}^{-1}\text{cm}^{-1}$ at 260 nm, $I = 0.10 \text{ M}$, pH = 7.0 [42]); concentrations of ct-DNA are expressed in molarity of base pairs. Polyriboadenylic·polyribourydylic (poly(A)·poly(U)) and polyribourydylic (poly(U)) acids were purchased from Sigma as potassium salts and the stock solutions were prepared by dissolving suitable amounts of the solid in water. The standardization

of the synthetic RNA stock solutions was attained spectrophotometrically ($\epsilon = 14900 \text{ M}^{-1}\text{cm}^{-1}$ at 260 nm for poly(A)·poly(U) and $\epsilon = 8900 \text{ M}^{-1}\text{cm}^{-1}$ at 260 nm for polyU, at $I = 0.1 \text{ M}$, $\text{pH} = 7.0$ [43]). Poly(U)·poly(A)□poly(U) was obtained at $\text{pH} = 7.0$ by the quantitative reaction between equimolar amounts of poly(U) and poly(A)·poly(U) [44]. The analytical concentration of poly(U), poly(A)·poly(U) and poly(U)·poly(A)□poly(U) are expressed in molarity of single bases, base pairs and base triplets respectively and indicated as C_U , C_{AU} and C_{UAU} respectively. For polynucleotides, the measurements were performed at 0.1 M NaCl and sodium cacodylate (NaCac) 2.5 mM ($\text{pH} = 7.0$ buffer). The dried DNA oligonucleotide Tel23 (hybrid) was purchased from Metabion. Its stock solution was prepared in an aqueous buffer containing 0.1 M KCl, 2.5 mM LiCac (lithium cacodylate, $(\text{CH}_3)_2\text{AsO}_2\text{Li}$) at $\text{pH} = 7.0$. The molar concentration (in strands) is calculated according to the weight/content provided by the sample certificate. The formation of the G-quadruplex (G4) structure was carried out by heating the solution up to 90°C for 6 min and slowly cooling down to room temperature. Doubly labelled oligonucleotides (fluorescein amidite FAM as 5'-donor and carboxytetramethylrhodamine TAMRA as 3'-acceptor, purchased from Eurogentec as dried samples) were prepared as $100 \mu\text{M}$ stock solutions in MilliQ water. $0.25 \mu\text{M}$ stock solutions were annealed in 10 mM KCl + 90 mM LiCl + 10 mM LiCac, $\text{pH} 7.4$, in order to obtain working solutions $0.2 \mu\text{M}$. The oligonucleotides' types and sequences are listed in Table 1. Ultra-pure grade water from a SARTORIUS Arium-pro water purification system was used as the reaction medium. All reactants not specifically mentioned were analytical grade and were used without further purifications.

Table 1. Biological role and sequences of the oligonucleotides used (lower part of the table refers to the tagged oligos with F = FAM and Ta = TAMRA fluorescent labels).

Name	G4 Type/origin	Tetrads	Sequence (5' to 3')
Tel23	hybrid DNA human telomere	3	TAGGGTTAGGGTTAGGGTTAGGG
dx	DNA intramolecular duplex	3	F-TATAGCTAT-hexaethyleneglycol-TATAGCTATA-Ta
Tel21	hybrid DNA human telomere	3	F-GGGTTAGGGTTAGGGTTAGGG-Ta
RTel21	parallel RNA human telomere	3	F-GGGUUAGGGUUAGGGUUAGGG-Ta
CEB25	parallel DNA minisatellites	3	F-AAGGGTGGGTGTAAGTGTGGGTGGGT-Ta
CTA21	antiparallel DNA human telomere	3	F-GGGCTAGGGCTAGGGCTAGGG-Ta
TBA	antiparallel DNA aptamer	2	F-GGTTGGTGTGGTTGG-Ta
BOM17	antiparallel DNA <i>bombyx</i> telomere	2	F-GGTTAGGTTAGGTTAGG-Ta

2.2 Experimental methods The spectrophotometer is a UV-2450 from Shimadzu equipped a temperature control to within $\pm 0.1^\circ\text{C}$. In the titrations, increasing amounts of the titrant are added directly in the cuvette. The precise and accurate addition of small volumes of titrant is done owing to a glass syringe connected to a micrometric screw (Mitutoyo, 1 turn = $8.20 \mu\text{L}$). In the ethidium exchange experiments (EtBr, Sigma, $\epsilon = 5700 \text{ M}^{-1}\text{cm}^{-1}$ at 480 nm), ct-DNA is first saturated with EtBr producing the fluorescence emission signal typical of the intercalated probe ($\lambda_{\text{ex}} = 520 \text{ nm}$, $\lambda_{\text{em}} = 595 \text{ nm}$); then, the molecule to be tested is added to the EtBr/ct-DNA mixture and a strong fluorescence decrease is taken as the proof of EtBr displacement by the intercalating species [45]. Circular dichroism (CD) spectra are recorded on a MOS-450 spectrophotometer (Bio-Logic SAS, Claix,

France) at 25.0 °C in a 1.0 cm cell. A buffer baseline is collected and subtracted from the sample spectra. The ITC experiments are performed with a Nano ITC (TA Instruments, Newcastle, USA). Working solutions are degassed for 30 min in a degassing station (TA, Waters LLC, New Castle, USA) to avoid the formation of bubbles during the titrations. The dye is injected (25 injections of 2.02 μL) directly into the calorimetric cell (187 μL) containing the polynucleotide solution in the buffer. The stirring speed is maintained constant at 250 rpm. For all ITC experiments, the contribution of the heat dilution of PZPERY is measured and subtracted from the titration data. The resulting thermograms (integrated area of the peak/mole of injectant versus [dye]/[polynucleotide] ratio) are treated with a model equation for an independent mode of binding using the Nano Analyze Software (TA Instruments, New Castle, USA). Fluorescence resonance energy transfer (FRET) melting experiments on G4s are carried out with a 7500 Real Time PCR System (Applied Biosystems). FAM fluorescence ($\lambda_{\text{exc}} = 492 \text{ nm}$, $\lambda_{\text{em}} = 516 \text{ nm}$) is recorded from 25°C to 95°C every 0.4°C at 1°C/min melting rate. 8-well optical tube strips are filled with 25 μL each well (20 μL G4 + 5 μL PZPERY). Normalised FAM fluorescence is plotted against temperature and the sigmoidal fit of the results provided the melting temperature (T_m) as the inflexion point of the curve. The difference between the T_m of PZPERY+G4 and the T_m of G4 represents the ΔT_m value. H₂O was used as the negative control.

2.3 Computational methods - QM calculations All quantum mechanical calculations were performed by using the Gaussian 16 package [46]. In order to build the intercalated model, we started from the solution structure of another intercalated DNA, i.e. the NMR-derived structure of a DNA fragment intercalated with Thiazole Orange (PDB: 108D) [47]. Both PZPERY and the DNA fragments constituting the pockets were treated at the QM level. The models used in the calculations represent: (i) a single molecule of PZPERY in water solution (ii) a system where PZPERY is placed in the intercalation pocket of DNA [48]. All geometry optimizations were performed with PZPERY free to move. In the case of the intercalated system, all the DNA atoms were kept fixed. The Integral Equation Formalism (IEF) version [49] of the Polarizable Continuum Model (PCM) [50] was used to describe the solvent (water) both in the ground and in the excited state. PCM cavities were described as a series of interlocking spheres centred on atoms with universal force field (UFF) radii multiplied by a cavity size factor of 1.2. In the case of the intercalation pocket, a cavity size factor of 1.9 was used in order to fill the space between the base pairs in the double stranded DNA helix. Both absorption and emission energies in the PCM solvent were obtained within the corrected linear response (cLR) scheme [51]. Twenty starting structures were built for the intercalated system. These structures were screened through a preliminary optimization *in vacuo* at the PM6 semiempirical level. After removing redundant minima, the remaining structures were reoptimized at the B3LYP/6-31G(d) level of theory with the D3 dispersion corrections [52],[53]. The lowest-energy minimum was then chosen for the excited-state calculations. This procedure is used to remove the bias coming from the initial structure in determining the energy minimum [54]. The excited state geometries and the absorption and emission energies were calculated with the CAM-B3LYP functional and the 6-31+G(d) basis set. In the case of the intercalated system, the excited state optimizations were performed with the CAM-B3LYP functional using the 6-31+G(d) basis set to describe PZPERY and the 6-31G basis set for the DNA structure. Natural Transition Orbitals [55] (NTO) were calculated in order to analyse the nature of the transitions. The absorption line-shape of PZPERY and perylene diimide

was computed in the linear vibronic coupling approximation. A normal-mode analysis of PZPERY *in vacuo* was performed at the B3LYP/6-31G(d) level, followed by a gradient calculation for the excited state at the CAM-B3LYP/6-31G(d) level. The excited-state gradient was projected onto the normal modes to finally obtain the Huang-Rhys factors. The latter were used to finally compute the absorption line-shape in the second-order cumulant expansion formalism [56].

2.4 Computational methods – MD simulations

The structure of the Tel23 G-quadruplex in K⁺/water solution was obtained from the Protein Data Bank (PDB), with PDB id 2JPZ. In detail, the first, the second and the last residues of the G4 chain of the PDB file (a 26-mer hybrid) were removed and two K⁺ atoms were added between the tetrads by using the Maestro software (Maestro, version 10.2, Schrödinger, LLC, New York, NY, 2015), in order to generate the same Tel23 sequence of the experimental studies. The starting molecular structure of PZPERY was obtained by full geometry optimization through DFT calculations, as reported above. The starting structures of the PZPERY/Tel23 system were obtained by docking the ligand on the G4 host with the DOCK6 software [57]. Spheres within a radius of 0.14 – 0.4 nm were used to define the binding site into a 1.2 nm large box. The grid-based score depends on the non-bonded terms of the molecular mechanics force field. The ligand charge for the docking was calculated using the AM1-BCC method. For MD simulations, GAFF parameters were used for PZPERY, and the corresponding atom-types were assigned with the ACPYPE software (Antechamber PYthon Parser interface) [58],[59]. The Amber99SB force field ParmBSC1 nucleic acid parameters were used for the G4 model [60]. Atomic partial charges of PZPERY were obtained as RESP charges by Hartree-Fock (HF/6-31G(d)) calculations and using the Antechamber package. A triclinic box (1.0 nm depth on each side) of TIP3P water was generated around the PZPERY/Tel23 system, for a total of about 5500 solvent molecules; 39 K⁺ ions and 17 Cl⁻ ions were added to neutralize the negative charges of the G4 sugar-phosphate backbone and to set the solution ionic strength to approximately 0.15 M. Explicit solvent MD simulations for the PZPERY/G4 system were performed by using the Gromacs 5.0.4 software package [61],[62], at 300 K in the canonical NPT ensemble (whose number of particles (N), pressure (P) and temperature (T) are constant), under control of a velocity-rescaling thermostat [63]. The particle Mesh-Ewald method was used to describe long-range interactions [64]. Preliminary energy minimizations were run for 5000 steps with the steepest descent algorithm, followed by a 500 ps equilibration step, in which solute was harmonically restrained with a force constant of 1000 kJ/mol·nm², gradually relaxed in five consecutive steps of 100 ps each, to 500, 200, 100 and 50 kJ/mol·nm². The final production run of 100 ns (200 ns for binding site II) was performed without restraints. Root Mean Square Deviation (RMSD) plots were used to assess the stability of the G4 model and of the binding site. Clustering analysis was performed with the g-cluster tool to determine the most recurrent structures at equilibrium.

Binding energy calculations were performed with the MM/GBSA and MM/PBSA methods, which combine MM potentials with Generalized Born (GB) or Poisson-Boltzmann (PB) continuum calculations with surface area (SA) terms to compute energies of the complex, the ligand, and the DNA [65],[66],[67]. These calculations were performed with the MMPBSA.py [68] interface of *AmberTools 18* [69]. For MM/GBSA calculations, we used the GB model by Onufriev et al. [70] (option *igb* = 5 in Amber) in combination with the modified Bondi radii. We did not compute the entropic term of the interaction; therefore we will refer to the results as “binding enthalpies”. The

MM/PB(GB)SA calculations were performed on 600 frames extracted from the last 50 ns of each trajectory.

3. Results and discussion

3.1 PZPERY preliminary solution tests Before any subsequent test, the solution properties of PZPERY at physiological conditions (NaCl 0.1 M, NaCac 2.5 mM, pH 7.0) were measured. Absorbance spectra at different dye concentrations were recorded (Figure S1A – Supporting Information). Upon increasing concentrations, the absorbance profile changes and the absorbance ratio plots against C_{PZPERY} are not constant (Figure S1B). The well resolved shape with three peaks typical of PDIs monomers is never observed, in agreement with the presence of auto-aggregation phenomena [71],[72],[73],[74][75]; this behaviour is indicative of the formation of superimposed aggregates of the H-type [1],[76]. Aggregation was not observed by Isothermal Titration Calorimetry with 3.0 and 1.0 mM of PZPERY in the syringe. It may occur that the PZPERY self-aggregation features do not enable the calorimetric study [77].

3.2 Spectrophotometric and circular dichroism experiments Starting from the binding to polynucleotides, Figure 2 shows the absorbance spectra recorded during a spectrophotometric titration where known amounts of ct-DNA were added to a PZPERY solution.

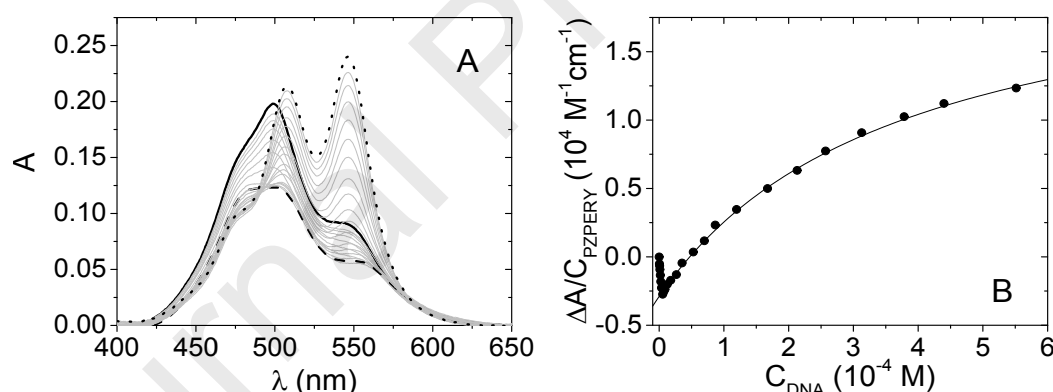


Figure 2. (A) Spectrophotometric titration of PZPERY/ct-DNA and (B) relevant binding isotherm at $\lambda = 550$ nm; $C_{\text{PZPERY}} = 1.16 \times 10^{-5}$ M, C_{DNA} from 0 (solid black line) to 5.57×10^{-4} M (dotted line), 37.0 °C, NaCl 0.1 M, NaCac 2.5 mM, pH 7.0. The spectrum corresponding to the minimum of the binding isotherm is evidenced as dashed line.

The spectral behaviour is biphasic and suggests that different binding features may apply to the two phases of the titration, namely in the presence of different reactants concentrations. The first phase (very first points of the titration) shows a signal decrease. It corresponds to dye excess conditions (high dye/DNA ratio). Such biphasic binding isotherms are non-rarely found for other systems also, and the first phase is explained on the basis of dye-dye interactions on the DNA surface [78][79]. PZPERY, which is already prone to aggregate when alone in solution, will be attracted by the (negatively charged) DNA backbone and produce a locally high concentration of molecules.

Therefore, the dye will even more aggregate on the DNA surface, likely favouring some cooperative external binding over monomer intercalation. This cooperative external binding is not likely to occur in some real system where the drug/probe ratio is low. In the second phase, the ct-DNA content increases, and the dye would dilute itself over a high quantity of polynucleotide's binding sites. Under these circumstances, aggregates break and the monomer can bind to DNA. This monomer binding process is the more interesting and probable from a biochemical point of view, and is that on which we focus. The loss of aggregation is confirmed by the rise of well resolved bands, peaked at ca. 485, 510 and 550 nm, which very much resemble the spectrum of PDI monomers (see below theoretical calculations and [1],[71][72]). The second branch of titration, where $C_{\text{DNA}}/C_{\text{PZPERY}} > 1$, can thus be fitted according to Eq. (1) to yield an estimate of the apparent binding constant of the monomer (K_{app}). It can be demonstrated that this procedure enables the good representation of the binding features even in the presence of auto-aggregation processes [79].

$$\Delta A/C_{\text{PZPERY}} = (K_{\text{app}}\Delta\epsilon[\text{DNA}])/(1+K_{\text{app}}[\text{DNA}]) + k \quad (1)$$

In this equation, $\Delta A = A - \epsilon_{\text{PZPERY}}C_{\text{PZPERY}}$ is the amplitude of the binding isotherm, $\Delta\epsilon = \epsilon_{\text{PZPERY}/\text{DNA}} - \epsilon_{\text{PZPERY}}$ is the difference of the molar extinction coefficients between bound and unbound forms, $[P]$ is the free DNA, and k is an offset. In the first step, $[\text{DNA}] = C_{\text{DNA}}$ (total ct-DNA molar concentration) is set to obtain a first K_{app} estimation which is used to re-calculate $[\text{DNA}] = C_{\text{DNA}} - [\text{PZPERY}/\text{DNA}]$. The procedure is repeated until convergence is reached. We obtain $K_{\text{app}} = (2.8 \pm 0.9) \times 10^3 \text{ M}^{-1}$ at 37.0°C. The titration is repeated at different temperatures. No significant dependence of K_{app} on temperature is observed (Figure S2), likely due to some enthalpy compensation between endothermic dis-aggregation and exothermic DNA binding processes. Figure S3 shows that the interaction is favoured at lower ionic strength (steeper second branch) in agreement with the electrostatic attraction between the DNA phosphate groups and the positive PZPERY. These experiments also evidence changes in the absorbance shape of PZPERY at different salt content which confirm the different extent of auto-aggregated forms. Ionic strength increase is known to promote PDI's intermolecular interactions [25]: in agreement with previous observations, the absorbance profile is less resolved at NaCl 1.0 M + NaCac 2.5 mM with respect to NaCac 2.5 mM only. The binding to RNAs is different with respect to ct-DNA, both for poly(A)·poly(U) duplex and poly(U)·poly(A)□poly(U) triplex which behave in a similar way. Under the same experimental conditions, the signal change upon binding is still evident but much more limited and the second branch of the titration cannot reach a curvature (Figure S4). Therefore, K_{app} could not be robustly evaluated for RNAs. Circular Dichroism (CD) titrations confirm the different behaviour of double-helix DNA vs. double- and triple-helix RNA (Figure 3).

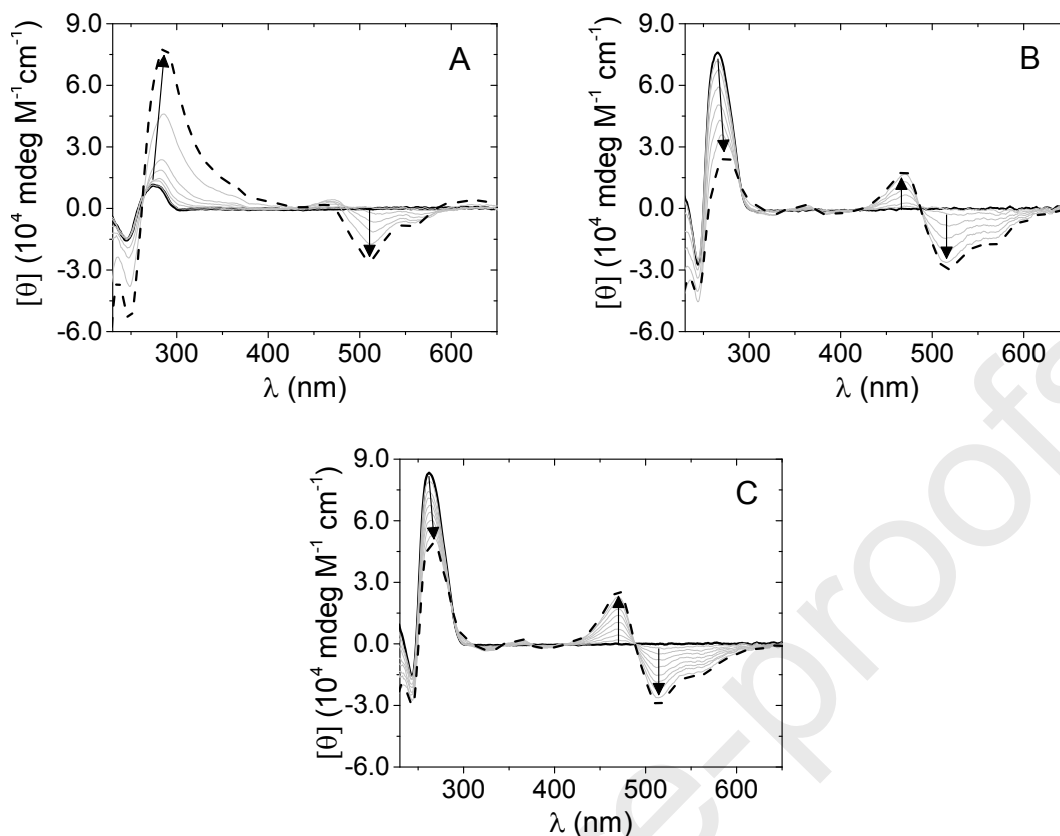


Figure 3. CD spectra of (A) PZPERY/ct-DNA ($C_{\text{DNA}} = 7.00 \times 10^{-5}$ M, C_{PZPERY} from 0 (no ICD signal) to 6.97×10^{-5} M (dashed line)); (B) PZPERY/polyA·polyU ($C_{\text{AU}} = 4.03 \times 10^{-5}$ M, C_{PZPERY} from 0 to 4.03×10^{-5} M); (C) PZPERY/poly(U)·poly(A)□poly(U) ($C_{\text{UAU}} = 6.50 \times 10^{-5}$ M, C_{PZPERY} from 0 to 8.03×10^{-5} M). NaCl 0.1 M, NaCac 2.5 mM, pH 7.0, 25.0°C. Arrows underline the changes occurring upon increasing PZPERY content.

The addition of increasing amounts of PZPERY to a ct-DNA solution provides a strong negative induced signal (ICD) in the visible part of the spectrum and a significant distortion of the CD bands of the DNA base pairs in the UV-range, suggesting intercalation of PZPERY into the polynucleotide [80]. Intercalation of a dye does not always generate an ICD band (in particular if the species does not have strong absorption bands in the visible range). However, the born of a strong ICD band means that the binding process induces a highly ordered geometry for the dye, obtained thanks to the coupling with the DNA template. The analysis of the sign and amplitude of the ICD band may confirm that this high order-inducing process is intercalation. The amplitude of the ICD signal corresponds to $\Delta\epsilon$. The maximum numerical value of $\Delta\epsilon$ can be calculated at the maximum ICD (508 nm) using the relationships $[\theta] = \theta / (C_{\text{DNA}} \cdot 10)$ and $\Delta\epsilon = \theta / (32980 \times C_{\text{DNA}} \times b) = [\theta] / 3298$, being θ the ellipticity read, $[\theta]$ the molar ellipticity and b the path length (equal to 1 cm) [81]. We have here that $[\theta] = -2.52 \times 10^4$ mdeg and, thus, $\Delta\epsilon = -7.7 \text{ M}^{-1}\text{cm}^{-1}$, which is compatible with an intercalative process ($|\Delta\epsilon| < 10 \text{ M}^{-1}\text{cm}^{-1}$ [80]). The ICD signature is very different in the case of RNAs: isodichroic points (absent for DNA) are present and an evident degenerate exciton coupling appears. An analogous behaviour has been previously observed in the few studies on other PDIs binding to double stranded

RNA [36],[37]. Here, the induced (ICD) positive and negative bands point out groove binding as PZPERY/RNA binding mode for both duplex and triplex RNAs. The UV bands reveal that the conformational changes induced in the polynucleotide structure by PZPERY are too profound to arise from a simple external binding. The UV signals are more difficult to analyse as they reflect the sum of the changes coming from the polynucleotide and those from the UV-part of the ICD signal of the dye. Still, in the case of ct-DNA, the molar ellipticity is found to increase, which is opposite to what found in the case of RNAs. A significant bathochromic shift in the band at around 270 nm is observed for all three systems (ct-DNA 13 nm > poly(A)·poly(U) 8 nm > poly(U)·poly(A)□poly(U) 5 nm); this shift is higher in the case of ct-DNA, in agreement with the higher distortion produced by intercalation. Note that blank tests confirmed no ICD/background signal for PZPERY alone in buffer (Figure S5). PZPERY intercalation into ct-DNA is confirmed also by ethidium (EtBr) displacements assays (Figure S6). PZPERY addition to the probe-saturated nucleic acid produces a dramatic decrease of the light emission due to intercalated EtBr indicating that an exchange reaction takes place and that the studied PDI substitutes the other dye from its location in the intercalation pocket. To compare the affinity towards G4s against polynucleotides and evaluate possible selectivity rules, we performed absorbance titrations with the Tel23 oligonucleotide at different temperatures (Figure 4) (see below at FRET studies the reason for the choice of this particular sequence). The relevance of the spectral changes immediately suggests a strong affinity for Tel23: the bands of the bound species are similar but much more prominent than in the DNA/RNAs cases.

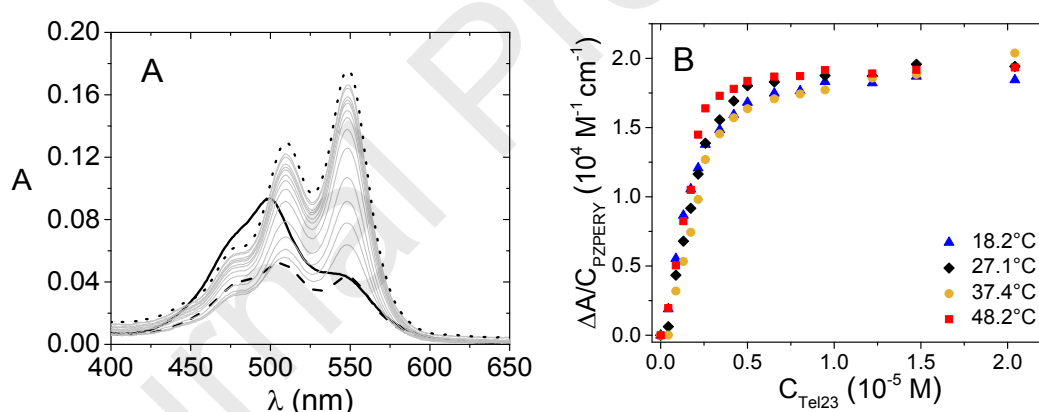


Figure 4. (A) Spectrophotometric titration of PZPERY/Tel23 ($C_{\text{PZPERY}} = 6.51 \times 10^{-6}$ M, C_{Tel23} from 0 (solid black line) to 2.04×10^{-5} M (dotted line), KCl 0.1 M, LiCac 2.5 mM, pH 7.0, 37.0°C) and (B) binding isotherms at different temperatures ($\lambda = 550$ nm). The spectrum corresponding to the minimum of the binding isotherm is evidenced as dashed line.

Over the whole analysed temperature range, the binding isotherms show the steep shape that is indicative of a quantitative reaction. This result agrees with the high selectivity shown for some PDIs for G4 structures [19]. The slope change occurs at $n = C_{\text{PZPERY}}/C_{\text{Tel23}}$ from 2 to 3, suggesting complex formation with stoichiometries higher than one.

CD titrations where increasing amounts of PZPERY are added to the G4 showed the born of a positive ICD band (Figure 5). This behaviour occurs only in the presence of dyes monomers bound on the lateral surface; oppositely, sitting atop positions would reflect in no ICD [82] whereas dye-dye interactions on the G4 would produce a bisignate ICD [25].

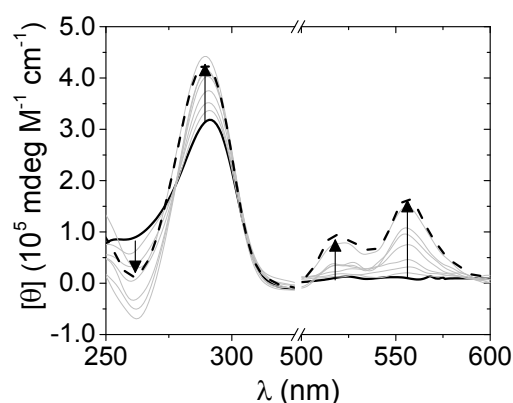


Figure 5. CD spectra of PZPERY/G4 ($C_{\text{Tel}} = 2.70 \times 10^{-6}$ M, C_{PZPERY} from 0 (no ICD signal, solid line) to 1.39×10^{-5} M (dashed line)); KCl 0.1 M, LiCac 2.5 mM, pH 7.0, 25.0°C. Arrows underline the changes occurring upon increasing PZPERY content.

3.3 Isothermal Titration Calorimetry (ITC) experiments The ITC experiments enable the determination of the thermodynamic parameters for the binding. The ITC profiles for ct-DNA, RNAs and Tel23 are very different (Figure 6). For ct-DNA and RNAs there is a specific binding process accompanied by non-specific binding processes that could be related to the PZPERY stacking along the polynucleotides. By contrast, the low dilution heat at the end of the Tel23 titration mean that in this case, non-specific binding processes are absent [83].

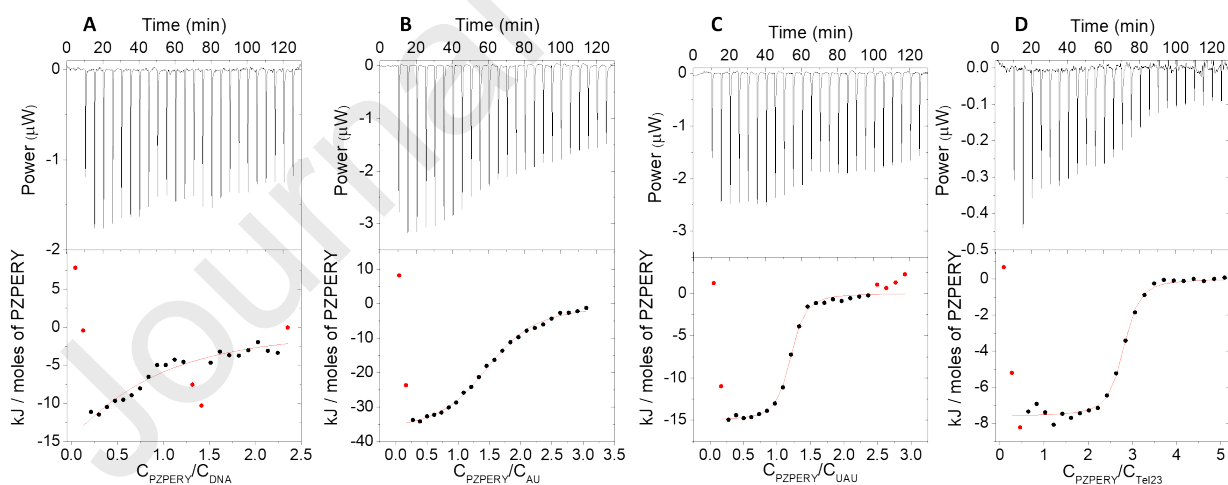


Figure 6. ITC titration with PZPERY of (A) ct-DNA, (B) poly(A)·poly(U), (C) poly(U)·poly(A)·poly(U) (for all tree $C^{\circ}_{\text{poly}} = 3.0 \times 10^{-4}$ M, $C^{\circ}_{\text{PZPERY}} = 3.0 \times 10^{-3}$ M, NaCl 0.1 M, NaCac 2.5 mM, pH 7.0, 25.0°C) and (D) Tel23 ($C^{\circ}_{\text{Tel23}} = 6.0 \times 10^{-5}$ M, $C^{\circ}_{\text{PZPERY}} = 3.0 \times 10^{-3}$ M, KCl 0.1 M, LiCac 2.5 mM, pH 7.0, 25.0°C). Upper panels = heat-flow profiles, lower panels = relevant thermograms fitted with Nanoanalyze software (in red, excluded outliers).

The thermodynamic parameters of the PZPERY interaction with the different substrates are collected in Table 2. Although all the binding reactions are exothermic processes, they are entropically driven probably due to hydrophobic interactions and desolvation [84]. The binding

constant of PZPERY/ct-DNA is too small to be accurately determined by ITC and all data related to this system should be considered as qualitative only. However, K value is in line with spectrophotometric results. PZPERY shows the greatest affinity towards the human telomeric G-quadruplex DNA and the lowest towards ct-DNA similarly to the well-known highly selective specific G4 ligands 360A-Br and PhenDC3 [85]. The positive charge of the two NH piperazinyl groups and the aromaticity of the perylene were the key for the thermal stabilization of G-quadruplex Tel23. The highest affinity of positively charged perylene derivatives towards G4 with respect to triplex or duplex DNA has been previously described [86],[87]. The $n = C_{\text{PZPERY}}/C_{\text{poly}} \neq 1$ value found in the case of Tel23 agrees with previous spectrophotometric findings.

Table 2. Thermodynamic parameters obtained by ITC for the interaction between PZPERY and the quoted biomolecules. NaCl 0.1 M, NaCac 2.5 mM for polynucleotides, KCl 0.1 M, LiCac 2.5 mM for Tel23, pH 7.0, 25°C.

	DNA ^a	poly(A)·poly(U)	poly(U)·poly(A)□poly(U)	Tel 23
K (M ⁻¹)	3×10^3	$(3.3 \pm 0.1) \times 10^4$	$(3.5 \pm 0.8) \times 10^5$	$(1.6 \pm 0.5) \times 10^6$
ΔH (kJ/mol)	-6	-6.1 ± 0.2	-2.5 ± 0.1	-3.8 ± 0.1
ΔS (J/mol·K)	47	65.9	97.8	108.9
n	0.9	1.5 ± 0.1	1.1 ± 0.1	2.7 ± 0.1

^a No accurate determination possible, qualitative only data.

3.4 Foster Resonance Energy Transfer (FRET) melting tests

FRET melting tests were done using 2-tetrad (TBA and BOM17) and 3-tetrad G4s (Tel21, RTel21, 21CTA, TBA, 25CEB). This set contains antiparallel (21CTA, TBA and BOM17), parallel (RTel21 and 25CEB) and mixed/hybrid (Tel21) conformations. The FRET melting experiments reveal thermal stabilization of G4s by PZPERY to a different extent, being the effect on double stranded DNA much lower with respect to what found for G4s (Figure 7). PZPERY thermally stabilized all 3-tetrads G4s in a greater extent than all the 2-tetrads G4s. Different factors may contribute to the stabilisation, but it can be speculated that such a behaviour agrees with a contribution of the length in the “groove-parallel” direction (extension of the lateral surface) in the binding features. Among 3-tetrad G4s, parallel ones are least stabilized. This pattern is similar to that reported by Freccero et al. for core extended naphthalene diimides [88]. The most stabilized G4s are the human telomeric G4, Tel21 (hybrid) and 21CTA (antiparallel), in fact, at $r = 10$ the melting temperature is beyond the limits of the technique. We decided to focus the detailed analysis of the binding features on hybrid DNA human telomeric sequences (Tel21/Tel23). The top G-tetrad stacked binding mode of PDI derivatives has already been elucidated in previous papers [31]. Highly exposed tetrads constitute a major binding site which may not always be the most likely to occur in reality. Different papers enlighten the importance of quadruplex-polymorphism [89],[90] and structural studies have shown that the hybrid-type intramolecular G4 structure is the major conformation formed in the human telomeric sequences [91]. On this basis, and given the experimental results, we found it interesting to focus our studies on the hybrid G4 conformations.

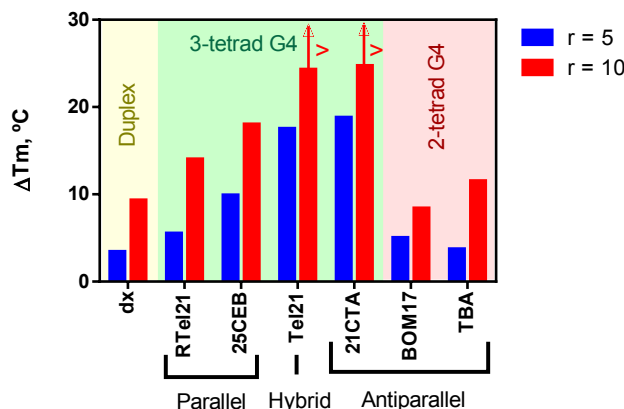


Figure 7. Values of ΔT_m obtained from FRET melting experiments. ΔT_m = difference in the melting temperature of the oligonucleotide with and without different concentrations of PZPERY, $r = [\text{PZPERY}]/[\text{G4}]$.

3.5 QM calculations for ct-DNA intercalation

Given that intercalation is found to be the active binding mode in the case of ct-DNA, we performed QM calculations in order to obtain a geometrical model of the complex. The ground-state geometries of the intercalated complex were obtained through a prescreening procedure with the PM6 semiempirical method, followed by optimizations at the DFT B3LYP-D3/6-31G(d) level (See Methods). This DFT approach was already used in previous studies by some of the authors to unravel the details of intercalation [48],[92],[54]. Because of the large size of the system, we consider the double stranded DNA intercalation pocket as a simplified model, which limits the interactions between PZPERY and the polynucleotide to the first neighbours [54],[93]. The DNA model is obtained by eliminating the entire backbone except for two adjacent base pairs (GC and AT) and the sugar-phosphate groups connecting those bases. Excited-state structures were optimized at the TD-DFT level with the CAM-B3LYP functional and the 6-31+G(d) basis set. The superimposition of the TD-DFT optimized structures of the ground (in blue) and the corresponding excited state (in green) (Figure 8) shows at a glance that they are essentially equivalent.

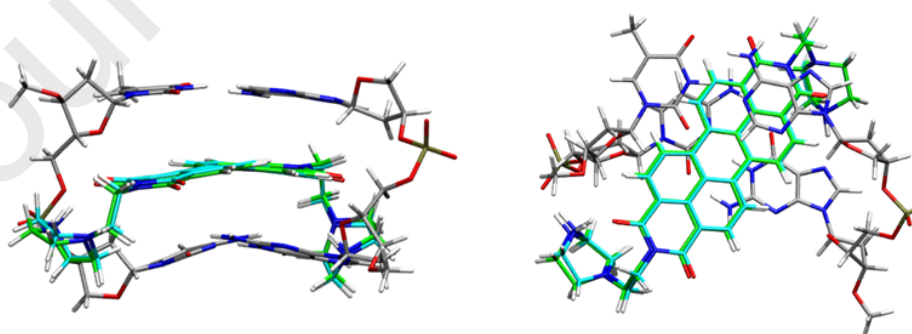


Figure 8. Ground state (blue) and excited state (green) optimized structures of PZPERY intercalated into the DNA double helix.

In the most favourable arrangement, the aromatic core of PZPERY establishes π -stacking interactions with ct-DNA base pairs, whereas the positively charged substituents lean towards the negative phosphate groups. The Natural Transition Orbitals (NTO) provide a qualitative

representation for the electronic transition density. The dominant NTO pair for the $S_0 \rightarrow S_1$ transition of the intercalated system (95% of contribution to the transition) is shown in Figure S7. The dihedral angles (carbon atoms 1-2-3-4;5-6-7-8 of Figure S8), dipole moments, absorption and emission energies obtained with the TD-DFT calculations are summarized in Table 3. The calculated excitation energies of PZPERY do not significantly change as a result of the DNA binding. Therefore, the significant spectral changes observed during the absorbance titrations can only be explained by simultaneous binding and dis-aggregation processes. In order to further confirm that the spectral features observed in isolated PZPERY should be ascribed to aggregation, we simulated the absorption spectrum of monomeric PZPERY, compared with its precursor PDI (Figure S9). The absorption spectrum of PZPERY is identical to that of its precursor PDI for both shape and position, meaning that the charged substituents do not affect the spectral shape [1]. In addition, the shape of the simulated spectrum is very similar to that obtained in large excess of ct-DNA, further confirming that the spectral changes observed upon binding reflect the dis-aggregation of the dye.

Table 3. Calculated properties for PZPERY solvated in water and intercalated into the DNA.

	water	DNA
Dihedral angle GS	-87; 92	81; -81
Dihedral angle EXC	-87; 92	84; -81
Dipole moment GS (D)	7.03	$\mu_{GS} > \mu_{EXC}$
Dipole moment EXC (D)	7.04	
Oscillator Strength	1.07	0.54
ABS (eV)	2.52	2.40
FLUO (eV)	2.19	2.12

3.6 MD simulations for G4 interaction The spectrophotometric FRET tests suggest the occurrence of an external binding mode to G4, but the actual position of the ligand is difficult to determine because of the complexity of the system. In principle, PZPERY could: (a) stack to the G4-tetrad (“tetrad-parallel” direction); (b) sit-atop the G4 by establishing π - π interactions with the bases in the loops (again “tetrad-parallel” direction); (c) interact with the quadruplex grooves mainly because of the electrostatic attraction between the positive substituents and the negatively charged sugar-phosphate backbone (“groove-parallel” direction). Preliminary docking calculations confirmed both (b) and (c) possibilities; given the choice of a hybrid conformation, where the G-tetrad is hindered by the loops, option (a) is here not probable and we will focus on the other alternatives. Also note that the ligand only very rarely intercalates within the G4 itself but rather stacks on the surface of the terminal G-tetrad, a binding mode that is sometimes classified as a threading intercalation in the case of G4s even if no intercalation really occurs [31]. Thus, the MD simulations were performed on hybrid Tel23, on the sitting-atop position (binding site I) as it shows the best grid score, and on the lateral position (binding site II) as it is the most frequently occurring structure. RMSD plots can be used to evaluate the stability of each binding site. RMSDs from the

first frame are reported in Figure 9 for binding site II (Figure S11A-B for binding site I), but the convergence to the final structure was determined also by considering the RMSDs from the last frame (Figures S10 and S11C-D). The RMSDs of Tel23 (especially for the G-tetrads and the backbone) indicate that the oligonucleotide core does not undergo significant conformational changes during the MD. The RMSD for PZPERY was calculated after aligning the guanine bases to the first frame, in order to measure the relative displacement of PZPERY in the reference frame of the G4 core.

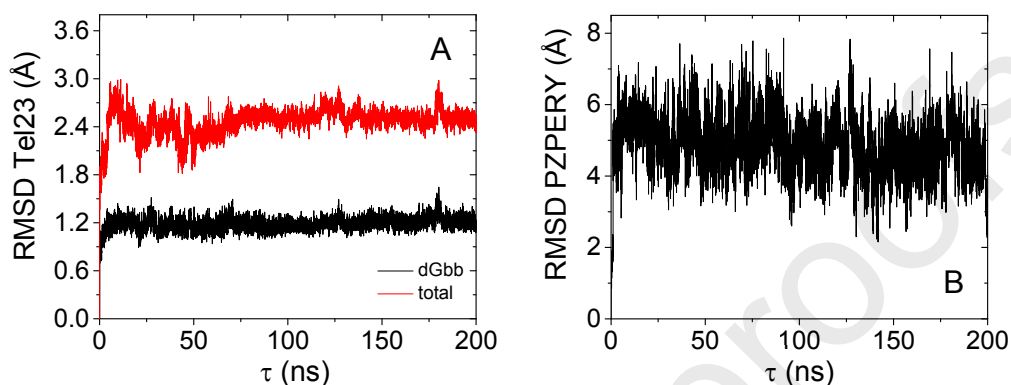


Figure 9. RMSD plots from the first frame for binding site II (lateral position - “groove-parallel” direction) related to (A) Tel23 (dGbb for guanine+backbone, in black; total for the entire structure, in red) and (B) PZPERY.

The RMSD analysis highlights that binding mode II is more flexible, as PZPERY is able to shift along the groove. However, the persistence of some H-bonds suggests that a precise arrangement of PZPERY is preferred. Table S2 reports the atoms involved in H-bonds together with the occurrence of the bond (as the fraction of frames in which the bond is formed with respect to the total MD frames) and the average distance between the donor and the acceptor atoms. On the contrary, for binding site I, no H-bond stabilizes the adduct. The high importance of hydrogen bonding in driving the different ability to interact with the G4 was already evidenced [27]. The stability of binding site II was characterized also by considering the distance between PZPERY and Tel23. Figure 10A shows that the distance (defined in Figure S12) between the ligand and the G4 residues remains approximately constant during the MD trajectory, showing a flexible but persistent binding mode.

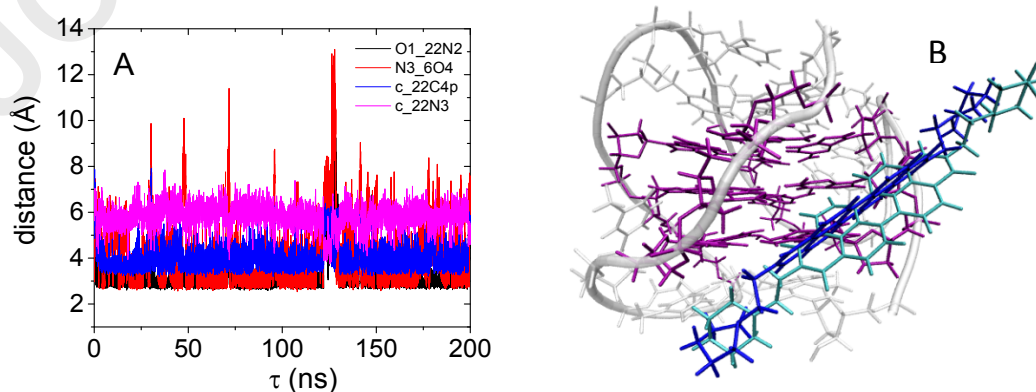


Figure 10. (A) Distance between Tel23 and PZPERY in binding site II (lateral position - “groove-parallel” direction - see Figure S12 for the definition of the distances); (B) PZPERY/Tel23 adduct for binding site II. Initial position coloured in blue, first cluster position in cyan.

In order to obtain a geometrical representation of the adducts, the PZPERY conformations explored in the last part of the MD (65 – 85 ns for binding site I, 150 – 170 ns for binding site II) were clustered with a cut-off of 0.2 nm. Figure 10B and Figure S13 represent the superimposition of the initial position of PZPERY (blue) and the one corresponding to a representative frame of the most populated cluster (cyan). Binding site II (lateral) could be stabilized by electrostatic attraction between the positively charged substituents and the negatively charged phosphate groups.

In order to estimate the relative stability of the two binding sites, we performed MM/PBSA and MM/GBSA calculations (See Computational Methods) for the binding enthalpy of the PZPERY to DNA along the two MD trajectories. The results (Table S1) show that binding site I (sitting-atop) has a ~9 kcal/mol greater binding enthalpy than binding site II (lateral), irrespective of the method employed. Analysis of the various MM/PB(GB)SA energy terms showed that the van der Waals MM term, common to both models, accounts for most of the difference between the two binding sites (Table S1). Indeed, binding site I is strongly favoured by the stacking interactions with flanking adenine nucleobases. It should be noted, however, that the force fields for nucleic acids tend to overestimate stacking interactions [94], thus we cannot regard these binding energies as quantitative. Nonetheless, the calculations show that both binding sites may be enthalpically favoured.

4. Conclusions

We have performed a combined spectroscopic/thermodynamic analysis of the interaction of a water soluble perylene diimide (PZPERY) to different biosubstrates. In parallel, theoretical calculations were also performed and were crucial to highlight the details of the adduct structures. This study widens the few examples on MD simulations for G4 binding and reports on a first DFT calculation on DNA/PDI derivatives.

PZPERY does bind to DNA and RNA polynucleotides but the affinity is not particularly high. The binding features are very different between DNA and RNAs as intercalation into calf-thymus DNA is found to occur, whereas groove binding is present for both double or triple RNAs. Natural calf thymus DNA is geometrically a B-DNA whereas poly(A)-poly(U) duplex resembles A-DNA with a deeper but narrower major groove and wider and shallower minor groove [95],[96],[97]; in the triplex the wide groove is furtherly hindered by the third strand. As often observed, the different geometries of the helices play a crucial role in driving the affinity towards a particular binding mode [79]. DFT calculations on the DNA adduct confirm that intercalation itself cannot produce the dramatic changes in the absorbance profiles of the dye which were experimentally observed. Therefore, this feature is due to the combined effect of intercalation and of aggregates disruption driven by monomer intercalation. When the negative enthalpy intercalation change [98] is balanced by the positive contribution of dis-aggregation [1],[72], the overall process has ΔH close to zero. The importance of the interplay between auto-aggregation and intercalation ability is quite straightforward and was already observed for neutral PDIs [99]. This is still present here for the

water-soluble +2 charged PZPERY: the negatively charged polynucleotides' backbone, in particular in the presence of a favourable geometry of the grooves may act as a template (see circular dichroism of RNAs).

PZPERY shows very good selectivity towards G4 tetrads. The MD simulations on a hybrid G4 form suggest that, in principle, both sitting-atop and lateral positions are possible. Planar ligands do often prefer the "tetrad-parallel" geometry for the adduct [30] and this process usually produces a strong G4 stabilisation [100] as it is observed by the FRET melting assays. On the other hand, MD also indicates the formation of H-bonds and very favourable complementary geometry for lateral binding, whereas the same is not found in sitting atop structures. FRET assays seem to suggest an increase in the stabilisation by increasing the "groove-parallel" direction (lateral surface). More robustly, the presence of ICD bands in the PZPERY/G4 system indicates lateral binding. Therefore, both experiments and calculation would show that the two binding modes are possible, with no significant preference of one over the other. Also, both spectrophotometric and ITC titrations agree with a binding stoichiometry higher than 2:1, indicating that multiple binding modes may be simultaneously present.

Acknowledgements

This contribution is based upon work from COST Action CA18202, NECTAR - Network for Equilibria and Chemical Thermodynamics Advanced Research, supported by COST (European Cooperation in Science and Technology). The authors gratefully acknowledge the financial support by "la Caixa" Foundation (LCF/PR/PR12/11070003), Ministerio de Ciencia, Innovación y Universidades-FEDER (RTI2018-102040-B-100) and Junta de Castilla y León-FEDER (BU305P18). LC acknowledges funding by the European Research Council, under the grant ERC-AdG-786714 (LIFETimes). Prof. Benedetta Mennucci is gratefully acknowledged for fruitful discussions.

References

- [1] Würthner, F. Perylene Bisimide Dyes as Versatile Building Blocks for Functional Supramolecular Architectures. *Chem. Commun.*, **2004**, *4*, 1564–1579.
- [2] Lian, X.; Ma, Z.; Zhang, Z.; Yang, J.; Sun, S.; Gu, C.; Liu, Y.; Ding, H.; Hu, J.; Cao, X.; Zhu, J.; Li, S.; Chen, W. An In-Situ Spectroscopy Investigation of Alkali Metal Interaction Mechanism with the Imide Functional Group. *Nano Res.*, **2020**, *13*, 3224–3229.
- [3] Hardin, B.E.; Snaith, H.J.; McGehee, M.D. The Renaissance of Dye-Sensitized Solar Cells. *Nature Photonics*, **2012**, *6*, 162–169.
- [4] Debije, M.G.; Verbunt, P.P.C. Thirty Years of Luminescent Solar Concentrator Research: Solar Energy for the Built Environment. *Advanced Energy Materials*, **2012**, *2*, 12–35.
- [5] Li, G.; Zhao, Y.; Li, J.; Cao, J.; Zhu, J.; Sun, X.W.; Zhang, Q. Synthesis, Characterization, Physical Properties, and OLED Application of Single BN-Fused Perylene Diimide. *J. Org. Chem.*, **2015**, *80*, 196–203.
- [6] Lin, K.Y.; Burke, A.; King, N.B.; Kahanda, D.; Mazaheripour, A.; Bartlett, A.; Dibble, D.J.; McWilliams, M.A.; Taylor, D.W.; Jocson, J.M.; Minary-Jolandan, M.; Gorodetsky, A.A.; Slinker, J.D. Enhancement of the Electrical Properties of DNA Molecular Wires through Incorporation of Perylenediimide DNA Base Surrogates. *Chempluschem*, **2019**, *84*, 416–419.
- [7] Biver, T.; Criscitiello, F.; Di Francesco, F.; Minichino, M.; Swager, T.; Pucci, A. MWCNT/Perylene Bisimide Water Dispersions for Miniaturized Temperature Sensors. *RSC Adv.*, **2015**, *5*, 65023–65029.
- [8] Donati, F.; Pucci, A.; Cappelli, C.; Mennucci, B.; Ruggeri, G. Modulation of the Optical Response of Polyethylene Films Containing Luminescent Perylene Chromophores. *J. Phys. Chem. B*, **2008**, *112*, 3668–3679.
- [9] Muniz-Miranda, F.; Minei, P.; Contiero, L.; Labat, F.; Ciofini, I.; Adamo, C.; Bellina, F.; Pucci, A. Aggregation Effects on Pigment Coatings: Pigment Red 179 as a Case Study. *ACS Omega*, **2019**, *4*, 20315–20323.
- [10] Minei, P.; Lessi, M.; Contiero, L.; Borsacchi, S.; Martini, F.; Ruggeri, G.; Geppi, M.; Bellina, F.; Pucci, A. Boosting the NIR Reflective Properties of Perylene Organic Coatings with Thermoplastic Hollow Microspheres: Optical and Structural Properties by a Multi-Technique Approach. *Sol. Energy*, **2020**, *198*, 689.
- [11] Hu, Y.; Han, D.; Zhang, Q.; Wu, T.; Li, F.; Niu, L. Perylene Ligand Wrapping G-Quadruplex DNA for Label-Free Fluorescence Potassium Recognition. *Biosens. Bioelectron.*, **2012**, *38*, 396–401.
- [12] Hu, R.; Liu, T.; Zhang, X.B.; Huan, S.Y.; Wu, C.; Fu, T.; Tan, W. Multicolor Fluorescent Biosensor for Multiplexed Detection of DNA. *Anal. Chem.*, **2014**, *86*, 5009–5016.
- [13] Deng, H.M.; Zhu, M.H.; Huang, L.J.; Chai, Y.Q.; Liu, X.R.; Yuan, R.; Yuan, Y.L. Novel D-A-D-Type Supramolecular Aggregates with High Photoelectric Activity for Construction of Ultrasensitive Photoelectrochemical Biosensor. *Anal. Chem.*, **2019**, *91*, 12468–12475.
- [14] Hu, R.; Zhang, X.; Xu, Q.; Lu, D.Q.; Yang, Y.H.; Xu, Q.Q.; Ruan, Q.; Mo, L.T.; Zhang, X.B. A Universal Aptameric Biosensor: Multiplexed Detection of Small Analytes via Aggregated Perylene-Based Broad-Spectrum Quencher. *Biosens. Bioelectron.*, **2017**, *92*, 40–46.
- [15] Rehm, T.H.; Stojković, M.R.; Rehm, S.; Škugor, M.; Piantanida, I.; Würthner, F. Interaction of Spermine-Alanine Functionalized Perylene Bisimide Dye Aggregates with Ds-DNA/RNA Secondary Structure. *Chem. Sci.*, **2012**, *3*, 3393–3397.
- [16] Xu, Z.; Guo, K.; Yu, J.; Sun, H.; Tang, J.; Shen, J.; Müllen, K.; Yang, W.; Yin, M. A Unique Perylene-Based DNA Intercalator: Localization in Cell Nuclei and Inhibition of Cancer Cells and Tumors. *Small*, **2014**, *10*, 4087–4092.

- [17] Xu, Z.; Cheng, W.; Guo, K.; Yu, J.; Shen, J.; Tang, J.; Yang, W.; Yin, M. Molecular Size, Shape, and Electric Charges: Essential for Perylene Bisimide-Based DNA Intercalator to Localize in Cell Nuclei and Inhibit Cancer Cell Growth. *ACS Appl. Mater. Interfaces*, **2015**, *7*, 9784–9791.
- [18] Takada, T.; Ishino, S.; Takata, A.; Nakamura, M.; Fujitsuka, M.; Majima, T.; Yamana, K. Rapid Electron Transfer of Stacked Heterodimers of Perylene Diimide Derivatives in a DNA Duplex. *Chem. - A Eur. J.*, **2018**, *24*, 8228–8232.
- [19] Busto, N.; Calvo, P.; Santolaya, J.; Leal, J.M.; Guédin, A.; Barone, G.; Torroba, T.; Mergny, J.L.; García, B. Fishing for G-Quadruplexes in Solution with a Perylene Diimide Derivative Labeled with Biotins. *Chem. - A Eur. J.*, **2018**, *24*, 11292–11296.
- [20] Franceschin, M.; Pascucci, E.; Alvino, A.; D'Ambrosio, D.; Bianco, A.; Ortaggi, G.; Savino, M. New Highly Hydrosoluble and Not Self-Aggregated Perylene Derivatives with Three and Four Polar Side-Chains as G-Quadruplex Telomere Targeting Agents and Telomerase Inhibitors. *Bioorganic Med. Chem. Lett.*, **2007**, *17*, 2515–2522.
- [21] Kerwin, S.M.; Chen, G.; Kern, J.T.; Thomas, P.W. Perylene Diimide G-Quadruplex DNA Binding Selectivity Is Mediated by Ligand Aggregation. *Bioorganic Med. Chem. Lett.*, **2002**, *12*, 447–450.
- [22] Kern, J.T.; Kerwin, S.M. The Aggregation and G-Quadruplex DNA Selectivity of Charged 3,4,9,10-Perylenetetra-carboxylic Acid Diimides. *Bioorganic Med. Chem. Lett.*, **2002**, *12*, 3395–3398.
- [23] Rangan, A.; Fedoroff, O.Y.; Hurley, L.H. Induction of Duplex to G-Quadruplex Transition in the c-Myc Promoter Region by a Small Molecule. *J. Biol. Chem.*, **2001**, *276*, 4640–4640.
- [24] Haiyong, H.; Cliff, C.L.; Hurley, L.H. Accelerated Assembly of G-Quadruplex Structures by a Small Molecule. *Biochemistry*, **1999**, *38*, 6981–6986.
- [25] Rao, L.; Dworkin, J.D.; Nell, W.E.; Bierbach, U. Interactions of a Platinum-Modified Perylene Derivative with the Human Telomeric G-Quadruplex. *J. Phys. Chem. B*, **2011**, *115*, 13701–13712.
- [26] Rossetti, L.; Franceschin, M.; Bianco, A.; Ortaggi, G.; Savino, M. Perylene Diimides with Different Side Chains Are Selective in Inducing Different G-Quadruplex DNA Structures and in Inhibiting Telomerase. *Bioorganic Med. Chem. Lett.*, **2002**, *12*, 2527–2533.
- [27] Franceschin, M.; Lombardo, C.M.; Pascucci, E.; D'Ambrosio, D.; Micheli, E.; Bianco, A.; Ortaggi, G.; Savino, M. The Number and Distances of Positive Charges of Polyamine Side Chains in a Series of Perylene Diimides Significantly Influence Their Ability to Induce G-Quadruplex Structures and Inhibit Human Telomerase. *Bioorganic Med. Chem.*, **2008**, *16*, 2292–2304.
- [28] Summart, R.; Thaichana, P.; Supan, J.; Meepowpan, P.; Lee, T.R.; Tuntiwechapikul, W. Superiority of an Asymmetric Perylene Diimide in Terms of Hydrosolubility, G-Quadruplex Binding, Cellular Uptake, and Telomerase Inhibition in Prostate Cancer Cells. *ACS Omega*, **2020**, *5*, 29733–29745.
- [29] Rossetti, L.; Franceschin, M.; Schirripa, S.; Bianco, A.; Ortaggi, G.; Savino, M. Selective Interactions of Perylene Derivatives Having Different Side Chains with Inter- and Intramolecular G-Quadruplex DNA Structures. A Correlation with Telomerase Inhibition. *Bioorganic Med. Chem. Lett.*, **2005**, *15*, 413–420.
- [30] Han, H.; Langley, D.R.; Rangan, A.; Hurley, L.H. Selective Interactions of Cationic Porphyrins with G-Quadruplex Structures. *J. Am. Chem. Soc.*, **2001**, *123*, 8902–8913.
- [31] Fedoroff, O.Y.; Salazar, M.; Han, H.; Chemeris, V. V.; Kerwin, S.M.; Hurley, L.H. NMR-Based Model of a Telomerase-Inhibiting Compound Bound to G-Quadruplex DNA. *Biochemistry*, **1998**, *37*, 12367–12374.
- [32] Vincke, B.; Ghaoui, M.A.; Férey, N.; Martinez, X. Physical, Modular and Articulated Interface

- for Interactive Molecular Manipulation. *Sensors (Switzerland)*, **2020**, *20*, 1–17.
- [33] Li, M.H.; Luo, Q.; Xue, X.G.; Li, Z.S. Molecular Dynamics Studies of the 3D Structure and Planar Ligand Binding of a Quadruplex Dimer. *J. Mol. Model.*, **2011**, *17*, 515–526.
- [34] Collie, G.W.; Promontorio, R.; Hampel, S.M.; Micco, M.; Neidle, S.; Parkinson, G.N. Structural Basis for Telomeric G-Quadruplex Targeting by Naphthalene Diimide Ligands. *J. Am. Chem. Soc.*, **2012**, *134*, 2723–2731.
- [35] Guarra, F.; Marzo, T.; Ferraroni, M.; Papi, F.; Bazzicalupi, C.; Gratteri, P.; Pescitelli, G.; Messori, L.; Biver, T.; Gabbiani, C. Interaction of a Gold(i) Dicarbene Anticancer Drug with Human Telomeric DNA G-Quadruplex: Solution and Computationally Aided X-Ray Diffraction Analysis. *Dalt. Trans.*, **2018**, *47*, 16132–16138.
- [36] Rehm, T.H.; Stojković, M.R.; Rehm, S.; Škugor, M.; Piantanida, I.; Würthner, F. Interaction of Spermine-Alanine Functionalized Perylene Bisimide Dye Aggregates with Ds-DNA/RNA Secondary Structure. *Chem. Sci.*, **2012**, *3*, 3393–3397.
- [37] Gershberg, J.; Radić Stojković, M.; Škugor, M.; Tomić, S.; Rehm, T.H.; Rehm, S.; Saha-Möller, C.R.; Piantanida, I.; Würthner, F. Sensing of Double-Stranded DNA/RNA Secondary Structures by Water Soluble Homochiral Perylene Bisimide Dyes. *Chem. - A Eur. J.*, **2015**, *21*, 7886–7895.
- [38] Li, H.; Yue, L.; Wu, M.; Wu, F. Self-Assembly of Methylene Violet-Conjugated Perylene Diimide with Photodynamic/Photothermal Properties for DNA Photocleavage and Cancer Treatment. *Colloids Surfaces B Biointerfaces*, **2020**, *196*, 111351.
- [39] Donati, F.; Pucci, A.; Ruggeri, G. Temperature and Chemical Environment Effects on the Aggregation Extent of Water Soluble Perylene Dye into Vinyl Alcohol-Containing Polymers. *Phys. Chem. Chem. Phys.*, **2009**, *11*, 6276–6282.
- [40] Khalili, F.; Henni, A.; East, A.L.L. PKa Values of Some Piperazines at (298, 303, 313, and 323) K. *J. Chem. Eng. Data*, **2009**, *54*, 2914–2917.
- [41] Biver, T.; Aydinoglu, S.; Greco, D.; Macii, F. Mechanistic Details on Pd(II)/5,10,15,20-Tetrakis(1-Methyl-4-Pyridyl)Porphyrin Complex Formation and Reactivity in the Presence of DNA. *Monatshefte fur Chemie*, **2018**, *149*, 175–183.
- [42] Felsenfeld, G.; Hirschman, S.Z. A Neighbor-Interaction Analysis of the Hypochromism and Spectra of DNA. *J. Mol. Biol.*, **1965**, *13*, 407–427.
- [43] Biver, T.; Busto, N.; García, B.; Leal, J.M.; Menichetti, L.; Secco, F.; Venturini, M. Mg(II) and Ni(II) Induce Aggregation of Poly(RA)Poly(RU) to Either Tetra-Aggregate or Triplex Depending on the Metal Ion Concentration. *J. Inorg. Biochem.*, **2015**, *151*, 115–122.
- [44] Hoyuelos, F.J.; García, B.; Leal, J.M.; Busto, N.; Biver, T.; Secco, F.; Venturini, M. RNA Triplex-to-Duplex and Duplex-to-Triplex Conversion Induced by Coralyne. *Phys. Chem. Chem. Phys.*, **2014**, *16*, 6012–6018.
- [45] Jenkins, T.C. Optical Absorbance and Fluorescence Techniques for Measuring DNA-Drug Interactions. *Methods Mol. Biol.*, **1997**, *90*, 195–218.
- [46] Frisch, M.J.; Trucks, G.W.; Schlegel, H.E.; Scuseria, G.E.; Robb, M.A.; Cheeseman, J.R.; Scalmani, G.; Barone, V.; Petersson, G.A.; O., F.; Foresman, J.B.; Fox, J.D. *Gaussian 16. Gaussian, Inc., Wallingford CT, 2016.*
- [47] Spielmann, H.P.; Wemmer, D.E.; Jacobsen, J.P. Solution Structure of a DNA Complex with the Fluorescent Bis-Intercalator TOTO Determined by NMR Spectroscopy. *Biochemistry*, **1995**, *34*, 8542–8553.
- [48] Biancardi, A.; Biver, T.; Marini, A.; Mennucci, B.; Secco, F. Thiazole Orange (TO) as a Light-Switch Probe: A Combined Quantum-Mechanical and Spectroscopic Study. *Phys. Chem. Chem. Phys.*, **2011**, *13*, 12595–12602.
- [49] Cancès, E.; Mennucci, B.; Tomasi, J. A New Integral Equation Formalism for the Polarizable

- Continuum Model: Theoretical Background and Applications to Isotropic and Anisotropic Dielectrics. *J. Chem. Phys.*, **1997**, *107*, 3032–3041.
- [50] Tomasi, J.; Mennucci, B.; Cammi, R. Quantum Mechanical Continuum Solvation Models. *Chemical Reviews*, **2005**, *105*, 2999–3093.
- [51] Caricato, M.; Mennucci, B.; Tomasi, J.; Ingrosso, F.; Cammi, R.; Corni, S.; Scalmani, G. Formation and Relaxation of Excited States in Solution: A New Time Dependent Polarizable Continuum Model Based on Time Dependent Density Functional Theory. *J. Chem. Phys.*, **2006**, *124*, 124520.
- [52] Grimme, S.; Antony, J.; Ehrlich, S.; Krieg, H. A Consistent and Accurate Ab Initio Parametrization of Density Functional Dispersion Correction (DFT-D) for the 94 Elements H-Pu. *J. Chem. Phys.*, **2010**, *132*, 154104.
- [53] Grimme, S. Density Functional Theory with London Dispersion Corrections. *Wiley Interdiscip. Rev. Comput. Mol. Sci.*, **2011**, *1*, 211–228.
- [54] Macii, F.; Salvadori, G.; Bonini, R.; Giannarelli, S.; Mennucci, B.; Biver, T. Binding of Model Polycyclic Aromatic Hydrocarbons and Carbamate-Pesticides to DNA, BSA, Micelles and Liposomes. *Spectrochim. Acta - Part A Mol. Biomol. Spectrosc.*, **2019**, *223*, 117313.
- [55] Martin, R.L. Natural Transition Orbitals. *J. Chem. Phys.*, **2003**, *118*, 4775–4777.
- [56] S., M. Principles of Nonlinear Optical Spectroscopy. **1995**.
- [57] Moustakas, D.T.; Lang, P.T.; Pegg, S.; Pettersen, E.; Kuntz, I.D.; Brooijmans, N.; Rizzo, R.C. Development and Validation of a Modular, Extensible Docking Program: DOCK 5. *J. Comput. Aided. Mol. Des.*, **2006**, *20*, 601–619.
- [58] Wang, J.; Wolf, R.M.; Caldwell, J.W.; Kollman, P.A.; Case, D.A. Development and Testing of a General Amber Force Field. *J. Comput. Chem.*, **2004**, *25*, 1157–1174.
- [59] Wang, J.; Wang, W.; Kollman, P.A.; Case, D.A. Automatic Atom Type and Bond Type Perception in Molecular Mechanical Calculations. *J. Mol. Graph. Model.*, **2006**, *25*, 247–260.
- [60] Guy, A.T.; Piggot, T.J.; Khalid, S. Single-Stranded DNA within Nanopores: Conformational Dynamics and Implications for Sequencing; A Molecular Dynamics Simulation Study. *Biophys. J.*, **2012**, *103*, 1028–1036.
- [61] Van Der Spoel, D.; Lindahl, E.; Hess, B.; Groenhof, G.; Mark, A.E.; Berendsen, H.J.C. GROMACS: Fast, Flexible, and Free. *Journal of Computational Chemistry*, **2005**, *26*, 1701–1718.
- [62] Hess, B.; Kutzner, C.; Van Der Spoel, D.; Lindahl, E. GRGMACS 4: Algorithms for Highly Efficient, Load-Balanced, and Scalable Molecular Simulation. *J. Chem. Theory Comput.*, **2008**, *4*, 435–447.
- [63] Bussi, G.; Donadio, D.; Parrinello, M. Canonical Sampling through Velocity Rescaling. *J. Chem. Phys.*, **2007**, *126*, 0141001/1-014101/7.
- [64] Darden, T.; York, D.; Pedersen, L. Particle Mesh Ewald: An N-log(N) Method for Ewald Sums in Large Systems. *J. Chem. Phys.*, **1993**, *98*, 10089–10092.
- [65] Kollman, P.A.; Massova, I.; Reyes, C.; Kuhn, B.; Huo, S.; Chong, L.; Lee, M.; Lee, T.; Duan, Y.; Wang, W.; Donini, O.; Cieplak, P.; Srinivasan, J.; Case, D.A.; Cheatham, T.E. Calculating Structures and Free Energies of Complex Molecules: Combining Molecular Mechanics and Continuum Models. *Acc. Chem. Res.*, **2000**, *33*, 889–897.
- [66] Wang, E.; Sun, H.; Wang, J.; Wang, Z.; Liu, H.; Zhang, J.Z.H.; Hou, T. End-Point Binding Free Energy Calculation with MM/PBSA and MM/GBSA: Strategies and Applications in Drug Design. *Chem. Rev.*, **2019**, *119*, 9478–9508.
- [67] Hou, T.; Wang, J.; Li, Y.; Wang, W. Assessing the Performance of the MM_PBSA and MM_GBSA Methods. 1. The Accuracy. Pdf. *J. Chem. Inf. Model*, **2011**, *51*, 69–82.
- [68] Miller, B.R.; McGee, T.D.; Swails, J.M.; Homeyer, N.; Gohlke, H.; Roitberg, A.E. MMPBSA.Py:

- An Efficient Program for End-State Free Energy Calculations. *J. Chem. Theory Comput.*, **2012**, *8*, 3314–3321.
- [69] Lee, T.S.; Cerutti, D.S.; Mermelstein, D.; Lin, C.; Legrand, S.; Giese, T.J.; Roitberg, A.; Case, D.A.; Walker, R.C.; York, D.M. GPU-Accelerated Molecular Dynamics and Free Energy Methods in Amber18: Performance Enhancements and New Features. *J. Chem. Inf. Model.*, **2018**, *58*, 2043–2050.
- [70] Onufriev, A.; Bashford, D.; Case, D.A. Exploring Protein Native States and Large-Scale Conformational Changes with a Modified Generalized Born Model. *Proteins Struct. Funct. Genet.*, **2004**, *55*, 383–394.
- [71] Görl, D.; Zhang, X.; Würthner, F. Molecular Assemblies of Perylene Bisimide Dyes in Water. *Angewandte Chemie - International Edition*, **2012**, *51*, 6328–6348.
- [72] Würthner, F.; Chen, Z.; Dehm, V.; Stepanenko, V. One-Dimensional Luminescent Nanoaggregates of Perylene Bisimides. *Chem. Commun.*, **2006**, *4*, 1188–1190.
- [73] Wang, B.; Yu, C. Fluorescence Turn-on Detection of a Protein through the Reduced Aggregation of a Perylene Probe. *Angew. Chemie - Int. Ed.*, **2010**, *49*, 1485–1488.
- [74] Balakrishnan, K.; Datar, A.; Naddo, T.; Huang, J.; Oitker, R.; Yen, M.; Zhao, J.; Zang, L. Effect of Side-Chain Substituents on Self-Assembly of Perylene Diimide Molecules: Morphology Control. *J. Am. Chem. Soc.*, **2006**, *128*, 7390–7398.
- [75] Balakrishnan, K.; Datar, A.; Oitker, R.; Chen, H.; Zuo, J.; Zang, L. Nanobelt Self-Assembly from an Organic n-Type Semiconductor : Propoxyethyl-PTCDI. *J. Am. Chem. Soc.*, **2005**, *127*, 10496–10497.
- [76] Ruan, Y. Bin; Li, A.F.; Zhao, J.S.; Shen, J.S.; Jiang, Y.B. Specific Hg²⁺-Mediated Perylene Bisimide Aggregation for Highly Sensitive Detection of Cysteine. *Chem. Commun.*, **2010**, *46*, 4938–4940.
- [77] Freyer, M.W.; Lewis, E.A. Isothermal Titration Calorimetry: Experimental Design, Data Analysis, and Probing Macromolecule/Ligand Binding and Kinetic Interactions. *Methods in Cell Biology*, **2008**, *84*, 79–113.
- [78] Biver, T.; Boggioni, A.; Secco, F.; Turriani, E.; Venturini, M.; Yarmoluk, S. Influence of Cyanine Dye Structure on Self-Aggregation and Interaction with Nucleic Acids: A Kinetic Approach to TO and BO Binding. *Arch. Biochem. Biophys.*, **2007**, *465*, 90–100.
- [79] Macii, F.; Arnaiz, C.P.; Arrico, L.; Busto, N.; Garcia, B.; Biver, T. Alcian Blue Pyridine Variant Interaction with DNA and RNA Polynucleotides and G-Quadruplexes: Changes in the Binding Features for Different Biosubstrates. *J. Inorg. Biochem.*, **2020**, *212*, 111199.
- [80] Biver, T. Use of UV-Vis Spectrometry to Gain Information on the Mode of Binding of Small Molecules to DNAs and RNAs. *Appl. Spectrosc. Rev.*, **2012**, *47*, 272–325.
- [81] Berova, N.; Bari, L. Di; Pescitelli, G. Application of Electronic Circular Dichroism in Configurational and Conformational Analysis of Organic Compounds. *Chem. Soc. Rev.*, **2007**, *36*, 914–931.
- [82] White, E.W.; Tanious, F.; Ismail, M.A.; Reszka, A.P.; Neidle, S.; Boykin, D.W.; Wilson, W.D. Structure-Specific Recognition of Quadruplex DNA by Organic Cations: Influence of Shape, Substituents and Charge. *Biophys. Chem.*, **2007**, *126*, 140–153.
- [83] Funke, A.; Dickerhoff, J.; Weisz, K. Towards the Development of Structure-Selective G-Quadruplex-Binding Indolo[3,2-b]Quinolines. *Chem. - A Eur. J.*, **2016**, *22*, 3170–3181.
- [84] Chaires, J.B. Calorimetry and Thermodynamics in Drug Design. *Annual Review of Biophysics*, **2008**, *37*, 135–151.
- [85] Bončina, M.; Podlipnik, Č.; Piantanida, I.; Eilmes, J.; Teulade-Fichou, M.P.; Vesnaver, G.; Lah, J. Thermodynamic Fingerprints of Ligand Binding to Human Telomeric G-Quadruplexes. *Nucleic Acids Res.*, **2015**, *43*, 10376–10386.

- [86] Tuntiwechapikul, W.; Taka, T.; Béthencourt, M.; Makonkawkeyoon, L.; Randall Lee, T. The Influence of PH on the G-Quadruplex Binding Selectivity of Perylene Derivatives. *Bioorganic Med. Chem. Lett.*, **2006**, *16*, 4120–4126.
- [87] Vasimalla, S.; Sato, S.; Takenaka, F.; Kurose, Y.; Takenaka, S. Cyclic Perylene Diimide: Selective Ligand for Tetraplex DNA Binding over Double Stranded DNA. *Bioorganic Med. Chem.*, **2017**, *25*, 6404–6411.
- [88] Zuffo, M.; Guédin, A.; Leriche, E.D.; Doria, F.; Pirota, V.; Gabelica, V.; Mergny, J.L.; Freccero, M. More Is Not Always Better: Finding the Right Trade-off between Affinity and Selectivity of a G-Quadruplex Ligand. *Nucleic Acids Res.*, **2018**, *46*, 115.
- [89] Monchaud, D.; Teulade-Fichou, M.P. A Hitchhiker's Guide to G-Quadruplex Ligands. *Org. Biomol. Chem.*, **2008**, *6*, 627–636.
- [90] Lightfoot, H.L.; Hagen, T.; Tatum, N.J.; Hall, J. The Diverse Structural Landscape of Quadruplexes. *FEBS Letters*, **2019**, *593*, 2083–2102.
- [91] Yang, D.; Okamoto, K. Structural Insights into G-Quadruplexes: Towards New Anticancer Drugs. *Future Medicinal Chemistry*, **2010**, *2*, 619–646.
- [92] Biancardi, A.; Biver, T.; Secco, F.; Mennucci, B. An Investigation of the Photophysical Properties of Minor Groove Bound and Intercalated DAPI through Quantum-Mechanical and Spectroscopic Tools. *Phys. Chem. Chem. Phys.*, **2013**, *15*, 4596–4603.
- [93] Biancardi, A.; Burgalassi, A.; Terenzi, A.; Spinello, A.; Barone, G.; Biver, T.; Mennucci, B. A Theoretical and Experimental Investigation of the Spectroscopic Properties of a DNA-Intercalator Salphen-Type ZnII Complex. *Chem. - A Eur. J.*, **2014**, *20*, 7439–7447.
- [94] Chen, A.A.; García, A.E. High-Resolution Reversible Folding of Hyperstable RNA Tetraloops Using Molecular Dynamics Simulations. *Proc. Natl. Acad. Sci. U. S. A.*, **2013**, *110*, 16820–16825.
- [95] Neidle, S.; Pearl, L.H.; Skelly, J. V. DNA Structure and Perturbation by Drug Binding. *Biochem. J.*, **1987**, *243*, 1–13.
- [96] Wilson, W.D.; Ratmeyer, L.; Zhao, M.; Strekowski, L.; Boykin, D. The Search for Structure-Specific Nucleic Acid-Interactive Drugs: Effects of Compound Structure on RNA versus DNA Interaction Strength. *Biochemistry*, **1993**, *32*, 4098–4104.
- [97] Uno, T.; Hamasaki, K.; Tanigawa, M.; Shimabayashi, S. Binding of Meso-Tetrakis(N-Methylpyridinium-4-Yl)Porphyrin to Double Helical RNA and DNA·RNA Hybrids. *Inorg. Chem.*, **1997**, *36*, 1676–1683.
- [98] Chaires, J.B. A Thermodynamic Signature for Drug-DNA Binding Mode. *Arch. Biochem. Biophys.*, **2006**, *453*, 26–31.
- [99] Pivetta, C.; Lucatello, L.; Paul Krapcho, A.; Gatto, B.; Palumbo, M.; Sissi, C. Perylene Side Chains Modulate G-Quadruplex Conformation in Biologically Relevant DNA Sequences. *Bioorganic Med. Chem.*, **2008**, *16*, 9331–9339.
- [100] Lopes-Nunes, J.; Carvalho, J.; Figueiredo, J.; Ramos, C.I.V.; Lourenço, L.M.O.; Tomé, J.P.C.; Neves, M.G.P.M.S.; Mergny, J.L.; Queiroz, J.A.; Salgado, G.F.; Cruz, C. Phthalocyanines for G-Quadruplex Aptamers Binding. *Bioorg. Chem.*, **2020**, *100*, 103920.

HIGHLIGHTS

- PZPERY intercalates into DNA and binds the groove of triple/double RNA helices
- DFT calculations explain the spectrophotometric changes for DNA interaction
- PZPERY shows very good selectivity towards G4 tetrads over polynucleotides
- MD simulations enlighten details for both G4 sitting-atop and lateral bound forms
- If multiple bound forms are possible, FRET and CD suggest lateral one is preferred

